International Journal of Thermal Sciences 48 (2009) 1467–1476

Contents lists available at ScienceDirect

International Journal of Thermal Sciences

www.elsevier.com/locate/ijts

# Prediction of the thermal conductivity anisotropy of Si nanofilms. Results of several numerical methods

Damian Terris [a], Karl Joulain [a], Denis Lemonnier [a], David Lacroix [b,*], Patrice Chantrenne [c]

[a] LET, UMR 6608 CNRS, ENSMA, Université de Poitiers, B.P. 40109, 86960 Futuroscope Cedex, France
[b] LEMTA, Nancy Université, CNRS, B.P. 70239, 54506 Vandœuvre Cedex, France
[c] CETHIL, UMR 5008 CNRS, INSA-Lyon, Université Lyon 1, 69621 Villeurbanne Cedex, France

ARTICLE INFO

*Article history:*
Received 28 July 2008
Received in revised form 9 January 2009
Accepted 9 January 2009
Available online 3 February 2009

*PACS:*
63.20.-e
65.80.+n
02.60.Cb

*Keywords:*
Nanofilm
Silicon
Thermal conductivity
Numerical simulation

ABSTRACT

The purpose of this work is to predict the in-plane and cross-plane thermal properties of crystalline silicon films. Several thicknesses from 20 nm to 6 μm and mean temperatures between 20 and 500 K have been investigated. Heat transport properties in silicon films have been studied through three different techniques: a semi-analytical method based upon the Kinetic Theory, a deterministic solution of the Boltzmann Transfer Equation (BTE) through the Discrete Ordinate Method and a statistical handling of the BTE by means of Monte Carlo Method. Each technique requires a model for the bulk material dispersion curves and the collision times of the different scattering processes. The three techniques have been validated through their correct prediction of silicon bulk thermal conductivity. Comparisons with in-plane thermal conductivity calculations and measurements have been also discussed. Thus, the cross-plane thermal conduction properties have been predicted. The expected temperature and thickness variations of the thermal conduction properties have been observed: the cross-plane thermal conduction appears to be less efficient than the in-plane thermal conduction, which proves that a significant anisotropy exists.



## 1. Introduction

Nanotechnologies development is one of the major current issues in electronics. Transistors with nanometric sizes are now commonly accepted and already achieved in laboratories [1]. For such devices heat dissipation is a challenging problem that has to be solved [2,3]. Moreover, nanostructured technology improvement reaches limits for which the classical heat transfer laws are not valid [4]. Consequently, thermal properties of these nanostructured materials need to be known as their typical size goes down.

Cross-plane and/or in-plane thermal conductivity measurements have already been performed for superlattices [5–8] and single nanofilms [9–13]. Thermal conductivity exhibits a strong anisotropy in superlattices which is also expected for nanofilms. Nevertheless, these measurements are not numerous. Despite, thermal properties are key parameters for multilayered processor design. As a consequence, development of numerical tools aimed at the assessment of thermal properties in nanostructures has encountered a wide interest for semiconductors of various shapes (nanofilms, nanotubes, nanowires, ...).

In semiconductor crystals, solid state physics teaches us that heat flows through the lattice vibrations and heat carriers can be seen as quasi-particles called phonons. Historically, thermal conductivity in crystalline materials has been derived from the phonon mean free path [14], using the gas Kinetic Theory. Precursor studies by Klemens [15,16], Callaway [17] and Holland [18] have put into practice this method assuming the single relaxation time approximation to model the collision term occurring in the Boltzmann transport equation. With this formalism, boundary and impurity scattering as well as three phonon processes (normal and umklapp) contribute to a single relaxation time. The resulting models have successfully predicted the bulk thermal conductivity for various semiconductors (Si, Ge, with several dopant concentration) at low and high temperatures. One of the three methods used here is based on this approach and is semi-analytical [19]. This method is the fastest to implement. It easily gives values of the thermal conductivity. The other two methods are based upon the resolution of a transport equation (BTE). Majumdar [20] has developed such a phonon radiative transfer equation (PRTE) which is derived from the BTE introducing a phonon specific intensity through the multiplying factor $\mathbf{v}\hbar\omega\mathcal{D}(\omega)$ (where $\mathbf{v}$ is the phonon velocity in a given direction and $\mathcal{D}(\omega)$ the density of states). The PRTE can be solved by deterministic means such as those widely developed for neutron and photon propagation. Radiation numerical modeling tools [21,22] like the Discrete Ordinate Method (DOM), used in this

* Corresponding author.
*E-mail addresses:* Karl.Joulain@ensma.fr (K. Joulain), David.Lacroix@lemta.uhp-nancy.fr (D. Lacroix), patrice.chantrenne@insa-lyon.fr (P. Chantrenne).

1290-0729/$ – see front matter 
doi:10.1016/j.ijthermalsci.2009.01.005

**Nomenclature**

| | | |
|---|---|---|
| $C$ | volumic heat capacity | $\mathrm{J\,m^{-3}\,K^{-1}}$ |
| $\mathcal{D}$ | density of states | $\mathrm{m^{-3}\,J^{-1}}$ |
| $E$ | energy | J |
| $F$ | cumulative distribution function | |
| $g$ | degeneracy factor | |
| $G$ | thermal conductance | $\mathrm{W\,m^{-2}\,K^{-1}}$ |
| $\hbar$ | reduced Planck constant | $\mathrm{J\,s\,rad^{-1}}$ |
| $I$ | intensity | $\mathrm{W\,m^{-2}\,sr^{-1}}$ |
| $I^0$ | blackbody intensity | $\mathrm{W\,m^{-2}}$ |
| $k$ | thermal conductivity | $\mathrm{W\,m^{-1}\,K^{-1}}$ |
| $k_B$ | Boltzmann constant | $\mathrm{J\,K^{-1}}$ |
| $K$, $\mathbf{K}$ | wave vector | $\mathrm{m^{-1}}$ |
| $l$ | width | m |
| $L$ | thickness | m |
| $\mathbf{n}$ | surface normal | |
| $N$ | phonon number | |
| $p$ | polarization | |
| $P$ | probability | |
| $\dot{q}$ | heat flux | $\mathrm{W\,m^{-2}}$ |
| $R$ | radius | m |
| $\mathcal{R}$ | random number | |
| $t$ | time | s |
| $T$ | temperature | K |
| $\mathbf{u}$ | unit vector in the propagation direction | |
| $v_g$ | group velocity | $\mathrm{m\,s^{-1}}$ |
| $v_\varphi$ | phase velocity | $\mathrm{m\,s^{-1}}$ |
| $V$ | volume | $\mathrm{m^3}$ |
| $W$ | weighting factor | |

*Greek symbols*

| | | |
|---|---|---|
| $\kappa$ | phonon absorption coefficient | $\mathrm{m^{-1}}$ |
| $\mu, \eta, \xi$ | direction cosines | |
| $\rho$ | reflectivity | |
| $\tau$ | relaxation rate | s |
| $\theta, \phi$ | angular coordinates | rad |
| $\omega$ | angular frequency | $\mathrm{rad\,s^{-1}}$ |
| $\Omega$ | solid angle | sr |
| $\boldsymbol{\Omega}$ | propagation direction | |

*Subscripts*

| | |
|---|---|
| *BC* | boundary collision |
| *d* | defect |
| *L, LA* | longitudinal acoustic polarization |
| *ph* | phonon |
| *scat* | scattering |
| *T, TA* | transverse acoustic polarization |

work, are particularly well adapted to film [23] and wire geometries [24]. As computer performance has increased, other numerical methods have been developed to solve the BTE. Among them statistical approach is of interest since it can be used in complicated geometries and since it is also supposed to be more accurate as long as the number of sampled phonons remains large. Moreover, collision process is treated carefully at microscopic scale in this model. We have improved this technique [25] from the former works by Peterson [26], Mazumder and Majumdar [27] using the Monte Carlo Method (MCM).

The two methods based on the resolution of the BTE are much more difficult to implement and require more computational resources than the Kinetic Theory (KT) model. Nevertheless, the asset of using these methods is to get the temperature profile in the sample. Thus, one knows if the considered nanostructure is in the Fourier regime or if it reaches the ballistic regime, i.e. if the concept of thermal conductivity is relevant.

Eventually, Molecular Dynamic (MD) simulations have been more and more used to assess thermal conductivity [28,29]. In Molecular Dynamic simulations, the integration of the Newton law at the atomic scale can provide reliable values of the thermal conductivity, but only for high temperatures. At least, high enough so that the specific heat does not strongly depend on the temperature changing. For lower temperatures, a correction has to be applied in order to take into account specific heat variations. Actually, MD requires much more computation time than any other methods, so only small systems can be studied. Further, some MD simulations of silicon nanofilms have been used for comparisons.

The paper is organized in four parts. In the following section, each numerical method used to assess thermal conductivity in nanostructures is briefly recalled. Then, the three methods are validated through their correct prediction of the bulk silicon thermal conductivity. In Section 3, two methods (KT and DOM) and experimental measurements of the in-plane thin film conductivity are compared. We find that these methods give similar results for the in-plane silicon film thermal conductivity, close to experimental measurements. The three methods have been used to predict silicon nanofilm cross-plane conductance in Section 4. Several thicknesses and average temperatures have been tested. As the three methods still give similar results, we are confident in the prediction made for cross plane silicon films thermal properties for which no measurements have been performed up to now.

## 2. Numerical models for thermal conductivity

In this section the three numerical methods used in this work have been briefly recalled, the objective being to provide the key parameters of each technique. Besides, one can found extra information about these models in dedicated papers previously published. For each method, the parameters needed to perform thermal properties calculation are specified or referenced. These parameters are the vibration dispersion relations and the different scattering processes collision times. Note that these data can be different since the methods have been developed separately with different choices for the modeling of vibration properties. Concerning the dispersion relations, they are fitted from experimental measurements achieved by neutron scattering. Isotropy is assumed in the three models but the fits are not exactly the same although they are close enough to allow comparison of the modeled thermal properties. Concerning the vibration properties, different but close choices have also been made in order to retrieve the bulk silicon thermal properties. As it has been shown by Chung et al. [30], this is the correct combination between the relaxation times and dispersion curves that is essential in order to ensure a good modeling.

### 2.1. Model based on the kinetic theory of gas

This model has been developed to predict the thermal conductivity of nanostructures made of dielectric crystals. In such materials heat is transported through vibration modes. Quasi-particles, phonons, can be associated to the vibration modes. Thus, heat can be seen as the energy transported by phonons. In the case of a uniform distribution of phonon propagation direction, in a isotropic crystal, the Kinetic Theory (KT) of gas may be applied to predict the lattice thermal conductivity. Under these conditions, the ther-

mal conductivity $k_z$ in the direction $z$ associated to phonons of wave vector $\mathbf{K}$ and polarization $p$ can be written as [14,19,31]

$$k_z(\mathbf{K}, p) = C(\mathbf{K}, p) v_g^2(\mathbf{K}, p) \tau(\mathbf{K}, p) \cos^2\theta_z(\mathbf{K}) \tag{1}$$

where $v_g$ is the group velocity determined from the dispersion curves

$$v_g(\mathbf{K}, p) = \frac{d\omega(\mathbf{K}, p)}{d\mathbf{K}} \tag{2}$$

with $\omega$ the angular frequency. $\tau(\mathbf{K}, p)$ is the phonon relaxation time due to phonon scattering phenomena, $\theta_z(\mathbf{K})$ is the angle between the wave vector $\mathbf{K}$ and the direction $z$. $C(\mathbf{K}, p)$ is the specific heat per unit volume, namely the temperature derivative of the internal energy $U(\mathbf{K}, p)$. For a system of volume $V$ it can be written [14] with $x = \hbar\omega(\mathbf{K}, p)/k_B T$ as

$$C(\mathbf{K}, p) = \frac{k_B}{V} \frac{x^2 \exp(x)}{[\exp(x) - 1]^2} \tag{3}$$

The total thermal conductivity and specific heat are the sum of the individual contributions due to all the wave vectors $\mathbf{K}$ and polarizations $p$

$$k_z = \sum_{\mathbf{K}} \sum_{p} C(\mathbf{K}, p) v_g^2(\mathbf{K}, p) \tau(\mathbf{K}, p) \cos^2\theta_z(\mathbf{K}) \tag{4}$$

$$C = \sum_{\mathbf{K}} \sum_{p} C(\mathbf{K}, p) \tag{5}$$

Only the dispersion curves are required to calculate the bulk crystal specific heat. The wave vector sampling in the first Brillouin zone depends on the crystal shape. Silicon is composed of face cubic centered (FCC) elementary cells containing two atoms. Thus, there are 6 polarizations and then 6 dispersion curves for each wave vector direction. The crystal is completely defined by the number of cells $N_{a1}$, $N_{a2}$ and $N_{a3}$ in the direction of each primitive vector **a1**, **a2** and **a3**. Wave vectors describing the crystal vibrations are defined in the reciprocal space. They are the sum of

$$\mathbf{K}_{b1} = \frac{n_{a1}}{N_{a1}}\mathbf{b1}, \qquad \mathbf{K}_{b2} = \frac{n_{a2}}{N_{a2}}\mathbf{b2}, \qquad \mathbf{K}_{b3} = \frac{n_{a3}}{N_{a3}}\mathbf{b3} \tag{6}$$

where **bi** are **ai** reciprocal vectors. The limiting values of $n_{a1}$, $n_{a2}$ and $n_{a3}$ are such that the wave vectors belong to the first Brillouin zone of the primitive cell.

For the sake of simplicity, dispersion curves in [100] direction are used for all wave vector directions where $\mathbf{K}_{\max}$ is the largest wave vector of the first Brillouin zone. The dispersion curve model used here [19] allows to recover with a good accuracy the internal energy of silicon, by comparing the constant volume specific heat determined thanks to Eq. (5) with experimental results [32].

To calculate thermal conductivity, it is necessary to know the relaxation time, which depends on vibration mode frequency, temperature and system size. For a crystal, assuming that scattering mechanisms are not coupled (Matthiessen's rule), the expression describing the relaxation time can be written as

$$\tau^{-1}(\omega, p) = \tau_{ph-ph}^{-1}(\omega, p) + \tau_d^{-1}(\omega) + \tau_{BC}^{-1}(\omega, p) \tag{7}$$

$\tau_{ph-ph}^{-1}$ is the relaxation time due to phonon–phonon interactions including normal and umklapp processes. In this model the usual $\tau_{ph-ph}^{-1}$ expression [15–17,33], which depends on temperature, frequency and polarization reveals to be accurate enough to recover silicon thermal properties. Its general form being

$$\tau_{ph-ph}^{-1}(\omega) = A_p \omega^{\chi_p} T^{\xi_p} \tag{8}$$

The relaxation time due to phonon–defect interactions [34] is written as

$$\tau_d^{-1}(\omega) = A\omega^4 \tag{9}$$

Phonon boundary interactions have been also taken into account to calculate the total phonon relaxation time. Several expressions have been proposed for the relaxation time due to the system boundaries [34–36]. All of these are proportional to the relaxation time in the Casimir limit [37]. In this study, we consider the following expression [18]

$$\tau_{BC}^{-1}(\omega) = \frac{v_g(\omega, p)}{F L(\mathbf{K})} \tag{10}$$

$L(\mathbf{K})$ is the distance that a phonon can travel between two boundary surfaces in a considered wavevector direction $\mathbf{K}$. For thin films, the thickness of the film influences the thermal conductivity since the relaxation time due to phonon boundary surfaces is a function of the distance a phonon can travel between two free surfaces. Moreover, as the film thickness decreases, the number of wave vectors in the thickness direction also decreases, introducing the anisotropy of the thermal conductivity. Besides, $F$ mainly depends on the surface roughness.

Under the assumptions specified at the beginning of this section, thermal conductivity should be isotropic. Actually, in our KT model, Eq. (4) is still used when the phonon properties are not isotropic. This anisotropy might be due to the dispersion curve or to the relaxation time parameters. As it will be shown later, the thermal conductivity anisotropy has been taken into account through the relaxation time assessment.

All the parameters $A_p$, $B_p$, $A$, $F$, $\chi_p$ and $\xi_p$ have been determined in order to recover experimental silicon bulk thermal conductivity where the characteristic length is equal to $L(\mathbf{K}) = \mathcal{L} = 7.16 \times 10^{-3}$ m [18]. Different Umklapp relaxation times for longitudinal and transverse modes [18] have to be considered. For nearly pure silicon, the parameter $A$ mainly depends on the impurity concentration. Assuming that this concentration is fixed, $A$ is a constant which has already been defined [38]. All these parameters are recalled below, note that these parameters are different from the ones used by Holland since the relations used to fit the bulk conductivity are not exactly the same.

$$\begin{cases} A_T = 7 \times 10^{-13}\ \mathrm{K}^{-4},\ A_L = 3 \times 10^{-21}\ \mathrm{s\,K}^{-3/2} \\ \chi_T = 1,\ \xi_T = 4,\ \chi_L = 2,\ \xi_L = 3/2 \\ A = 1.32 \times 10^{-45}\ \mathrm{s}^3,\ F = 0.55 \end{cases} \tag{11}$$

It has been shown that the optical mode contribution remains lower than 3% of the thermal conductivity below 1000 K [19]. Besides, other studies point out the facts that optical phonons do not propagate energy within the medium [39] and are not interacting with acoustic ones if the temperature is not high enough [40]. Then, optical phonons have not been taken into account in this study.

### 2.2. Discrete ordinate method for the BTE

We now focus on the numerical calculation of thin film cross-plane conductive heat transfer by solving the BTE for phonons by means of the Discrete Ordinate Method (DOM). This technique proposed by Chandrasekhar [41] is a numerical tool that transforms the BTE into a set of simultaneous partial differential equation for each different propagation directions of carriers (photons, neutrons or phonons) [21]. The set of directions spans the total solid angle range of $4\pi$. Integrals over solid angle are approximated by numerical quadratures [42].

A specific spectral intensity $I_{\omega,p}(\mathbf{r}, \mathbf{u})$ [43] for phonons which depends on the angular frequency $\omega$, on the polarization branch $p$, on the location $\mathbf{r}$ and on direction $\mathbf{u}$ is introduced. The collision term into the Boltzmann equation is expressed in the frame of the relaxation time approximation. Under these conditions and in steady state, the BTE reads

$$\mathbf{u} \cdot \frac{\partial I_{\omega,p}(\mathbf{r}, \mathbf{u})}{\partial \mathbf{r}} + \kappa_{\omega,p} I_{\omega,p}(\mathbf{r}, \mathbf{u}) = \kappa_{\omega,p} I^0_{\omega,p}(\mathbf{r}) \tag{12}$$

This equation is similar to the so-called Radiative Transfer Equation (RTE). $\kappa_{\omega,p}$ is an equivalent phonon absorption coefficient and $I^0_{\omega,p}$ is an equilibrium phonon specific intensity. $I^0_{\omega,p}$ can be seen as the product of the phonon density of states, multiplied by the mean energy of a phonon at equilibrium temperature $T$, and by the group velocity over $4\pi$.

$$I^0_{\omega,p}(T) = \frac{\omega^2 d\omega}{2\pi^2 v^2_{\varphi\omega,p} v_{g\omega,p}} \times \frac{\hbar\omega}{\exp(\hbar\omega/k_B T) - 1} \times \frac{v_{g\omega,p}}{4\pi} \tag{13}$$

where $v_{g\omega,p}$ is the group velocity, $v_{\varphi\omega,p}$ the phase velocity, $\hbar$ the Planck constant and $k_B$ the Boltzmann constant. The equivalent phonon absorption coefficient can be expressed in terms of relaxation time $\kappa_{\omega,p} = 1/(v_{g\omega,p} \times \tau_{\omega,p})$ where $\tau_{\omega,p}$ is the total relaxation time.

BTE (12) has been solved for two different geometries: an in-plane configuration allowing the calculation of the in-plane thermal conductivity and a cross-plane configuration which provides the thin film cross-plane conductance. In both geometries boundary conditions for phonon reflection must be set. Reflection at crystal boundary can be specular, diffusive or partially specular and diffusive. In the most general situation where reflection occurs at position $\mathbf{r}$, the reflected specific intensity in direction $\mathbf{u}$ reads

$$I_{\omega,p}(\mathbf{r},\mathbf{u}) = \frac{\rho^d}{\pi} \int_{\mathbf{u}'\cdot\mathbf{n}<0} I_{\omega,p}(\mathbf{r},\mathbf{u}')|\mathbf{u}'\cdot\mathbf{n}|\, d\Omega' + \rho^s I_{\omega,p}(\mathbf{r},\hat{\mathbf{u}}) \tag{14}$$

where $\hat{\mathbf{u}}$ is the incident specular direction relatively to $\mathbf{u}$ and $\mathbf{u}'$ are the other incident directions. $d\Omega'$ is a part of solid angle associated to direction $\mathbf{u}'$. $\rho^d$ is the diffuse reflectivity and $\rho^s$ corresponds to the specular reflectivity.

In the in-plane configuration, we consider a thin film of height $L$ perpendicular to the $z$ direction, infinite in the $y$ direction and with a length $l \gg L$ in the $x$ direction. The system is therefore invariant in the $y$ direction. The phonon transport equation has been solved on a regular rectangular mesh in the $(x,z)$ plane. With the three direction cosines $(\mu,\eta,\xi)$ discretized equation (12) reads

$$\mu\frac{\partial I_{\omega,p}}{\partial x} + \xi\frac{\partial I_{\omega,p}}{\partial z} + \kappa_{\omega,p} I_{\omega,p} = \kappa_{\omega,p} I^0_{\omega,p} \tag{15}$$

At boundaries $x = 0$ and $x = l$, temperatures have been imposed. Thus, specific intensities at these boundaries are equal to the equilibrium specific intensity $I^0_{\omega,p}(T)$ at temperatures $T_0$ and $T_l$. At lateral boundaries $z = 0$ and $z = L$, a purely diffuse reflection condition has been set ($\rho^d = 1$ and $\rho^s = 0$). These boundary conditions have been depicted in Fig. 1 (top).

The cross-plane configuration has been obtained solving Eq. (12) in an axi-symmetric configuration with cylindrical coordinates. The phonon location becomes $\mathbf{r} = (x,\theta,z)$ and the phonon propagation direction $\mathbf{u}$ remains determined by the two angles $(\phi,\psi)$ or the three direction cosines $(\mu,\eta,\xi)$. The system is invariant under a rotation around the azimuthal angle $\theta$. The discretization domain is a cylinder with a radius $R$ and height $L$ along the $z$ direction. Temperatures have been imposed on $z = 0$ and $z = L$ boundaries. A specular reflection condition has been set in $r = 0$ due to the symmetry of the considered problem. In $r = R$, a specular reflection condition has been also set in order to ensure momentum conservation in the $z$ direction ($\rho^d = 0$ and $\rho^s = 1$). Thus, it simulates the heat transfer in the perpendicular direction of a thin film. These boundary conditions have been illustrated in Fig. 1 (bottom). Note that this axi-symmetric configuration can also predict the thermal behavior of a cylindrical nanowire if a purely diffuse reflection is set in $r = R$. With this axi-symmetric cylindrical geometry, BTE (12) becomes

$$\frac{\mu}{r}\frac{\partial(rI_{\omega,p})}{\partial r} - \frac{1}{r}\frac{\partial(\eta I_{\omega,p})}{\partial\phi} + \xi\frac{\partial I_{\omega,p}}{\partial z} + \kappa_{\omega,p} I_{\omega,p} = \kappa_{\omega,p} I^0_{\omega,p} \tag{16}$$

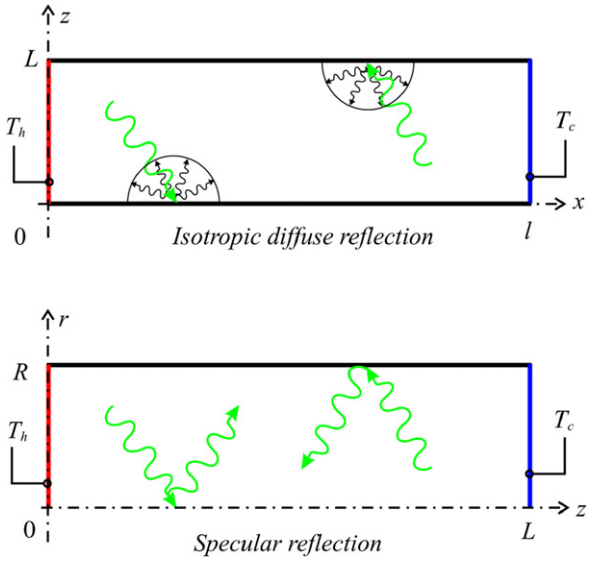


**Fig. 1.** Boundary conditions in the in-plane configuration (top) and the cross-plane configuration (bottom).

In both situations (in-plane and cross-plane), the angular integration has been performed for a given direction set. These directions have been chosen according to the $S_8$ quadrature [42] (80 directions spanning the total solid angle range of $4\pi$). The spatial discretization has been achieved in the bidimensional plane with regular mesh ($\approx 100 \times 100$ cells according to the modeled sample size).

Concerning the equivalent phonon absorption coefficient, different kinds of interactions have been taken into account through the global relaxation rate [18]. Interactions with impurities have been modeled by a Rayleigh scattering expression $\tau_d^{-1} = A\omega^4$. Normal anharmonic interaction have been characterized by $\tau_{NL}^{-1} = B_L\omega^2 T^3$ for longitudinal polarization and $\tau_{NT}^{-1} = B_T\omega T^4$ for transverse polarization. Umklapp anharmonic interaction has been described by $\tau_U^{-1} = B_{TU}\omega^2/\sinh(\hbar\omega/k_b T)$ at high transversal frequencies whereas $\tau_{UL}^{-1} = B_L\omega^2 T^3$ has been used for longitudinal polarization. The total inverse relaxation time has been obtained taking the sum of the inverse individual relaxation times (Matthiessen's rule). Constants $A$, $B_L$, $B_T$ and $B_{TU}$ used in the DOM simulation are those provided in [44]. Once again, only acoustic phonon modes have been considered. Calculations have proved that this is a satisfactory assumption to retrieve silicon thermal conductivity. Besides, crystal anisotropy has not been taken into account in the present study. The acoustic branches (*LA* and *TA*) of the dispersion properties have been modeled by a quadratic fit [45] of experimental data by Dolling [46] in the direction [100].

### 2.3. Monte Carlo method for the BTE

Monte Carlo (MCM) solution of the BTE is based upon energy considerations of the heat carrier interaction and displacement. Here, the studied domain has been spatially discretized in cubic cells where phonons have been allowed to drift and scatter (Fig. 2).

A uniform spectral discretization has been also achieved over $N_b$ frequency bands in order to take into account vibration properties through the dispersion curves. The random sampling technique requires a normalized distribution function $F(\omega,T)$. The later has been constructed computing the theoretical number of modes in each spectral band $\Delta\omega$ [25,27].

$$N_{b,p}(T) = V\left[\frac{1}{\exp\left(\frac{\hbar\omega_{b,p}}{k_B T}\right) - 1}\right]\frac{K^2_{b,p}}{2\pi^2 v_{gb,p}} g_p \Delta\omega \tag{17}$$

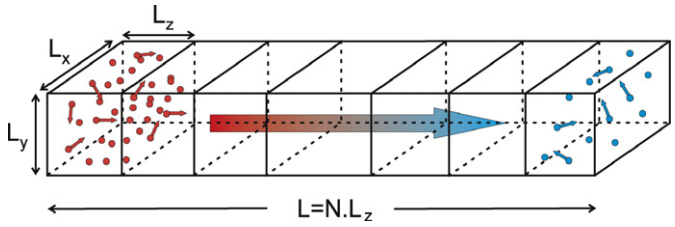


**Fig. 2.** Studied model. Phonons location, energy and velocity are randomly chosen in each cell according to dispersion curves and local temperature.

The indices $_{b,p}$ refer to band $b$ and polarization $p$, $g_p$ is the degeneracy of the polarization branch $p$. The distribution function $F$ has been constructed doing the cumulative summation of the number of phonons in the $i$th spectral band over the total number of phonons (Eq. (18))

$$F_i(T) = \frac{\sum_{b=1}^{i} \sum_p N_{b,p}(T)}{\sum_{b=1}^{N_b} \sum_p N_{b,p}(T)} \tag{18}$$

The number of modes $N$ for both polarizations and the corresponding distribution function $F$ are plotted on Fig. 3.

Thus, a random number $\mathcal{R}$ is sampled between 0 and 1, the corresponding $F_i(T)$ value gives the $i$th related spectral band with frequency center $\omega_i$. The phonon frequency is equal to

$$\omega = \omega_i + \frac{\Delta\omega}{2}(1 - 2\mathcal{R}) \tag{19}$$

The polarization has been also randomly set, calculating the probability to be or not on the $LA$ branch

$$P_{LA}(\omega_i) = \frac{N_{LA}(\omega_i, T)}{N_{LA}(\omega_i, T) + N_{TA}(\omega_i, T)} \tag{20}$$

The $n$th phonon location is randomly set in the considered cell $c$ at temperature $T$ using

$$\mathbf{r}_{n,c} = \mathbf{r}_c + L_x\mathcal{R}\,\mathbf{i} + L_y\mathcal{R}'\mathbf{j} + L_z\mathcal{R}''\mathbf{k} \tag{21}$$

where $\mathbf{r}_c$ is the coordinates of the cell of size $L_x \times L_y \times L_z$ and $\mathcal{R}$, $\mathcal{R}'$ and $\mathcal{R}''$ three random numbers. Eventually, the phonon propagation direction $\boldsymbol{\Omega}$ is determined choosing randomly a polar angle ($\cos(\theta) = 2\mathcal{R} - 1$) and an azimuthal angle ($\phi = 2\pi\mathcal{R}'$).

Phonons are drawn until the theoretical energy of the cell $E(T)$ (sum of every $E_{b,p}(T) = N_{b,p}(T) \times \hbar\omega_{b,p}$) reaches the assumed local equilibrium energy at temperature $T$. Actually, in the case of high temperature and/or for structures larger than some microns, the total theoretical number of phonons can be very large. On the other hand, as temperature goes down or in the case of very thin nanostructures the number of phonons can be insufficient to insure accurate statistics. Therefore, a weighting factor $W$ has been introduced to adjust numerically the number of sampled phonons and the energy of the medium. When $N(T)$ is large $W > 1$. At the opposite, if $N(T)$ is small we set $0 < W < 1$. Thus the resulting phonon density and energy become

$$N^\star(T) = \frac{N(T)}{W} \tag{22}$$

$$E^\star(T) = \sum_{n=1}^{N^\star(T)} W \times \hbar\omega_n \tag{23}$$

where $N^\star$ is the number of sampled phonons in a cell and $E^\star$ the corresponding energy. In practice, $W$ has been chosen so as to follow at least $10^4$ phonon in a 500 nm wide cubic cell. In this case, results are not sensitive to $W$ choice. The sampling process is stopped when $E^\star(T) = E(T)$. The model flow-chart is the following:

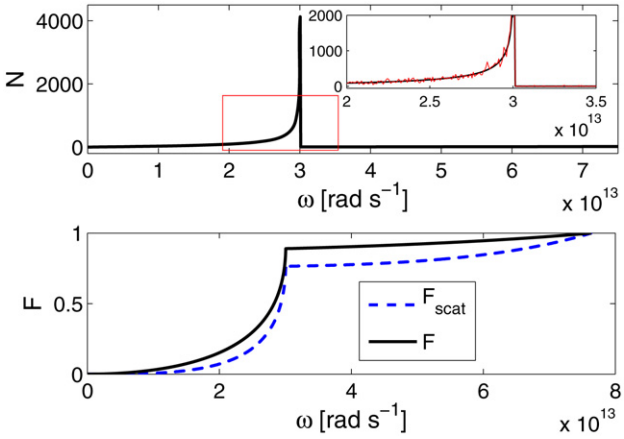


**Fig. 3.** Theoretical and sampled frequency phonon distribution at 300 K for silicon (upper figure). Normalized number density function in silicon with and without $P_{scat}$ correction (lower figure).

- According to the specified initial and boundary conditions (temperature set in the medium and at both sides of the film), phonons are randomly sampled (frequency, polarization and position) within each cell until the prescribe energy $E(T)$ is reached. Concerning film boundaries, the first and the last cells are blackbodies with fixed temperatures, i.e. after each time steps phonon distribution in these two cells is resampled according to the bounding hot and cold temperatures in order to maintain the temperature gradient.
- The energy transport process modeling is considered during $\Delta t$. Within a time step, phonons move according to their group velocity and direction propagation $\boldsymbol{\Omega}$. They can be reflected at a boundary of the domain and therefore change their propagation direction $\boldsymbol{\Omega}$ into $\boldsymbol{\Omega}'$ or travel toward a neighboring cell. In the case of specular reflection ($\rho^s = 1$ thus $\boldsymbol{\Omega}\cdot\mathbf{n} = -\boldsymbol{\Omega}'\cdot\mathbf{n}$). For diffuse reflection (depending on the rugosity) $\boldsymbol{\Omega}'$ is sampled in the backward angular space considering the normal $\mathbf{n}$ of the interaction surface.
- Following this drift stage, updated energies and temperatures are computed in every cells.
- Finally, some phonons can encounter a scattering process which depends on the relaxation time $\tau(\omega, p)$ and the simulation time step through the collision probability (Eq. (24)). In the case of a collision, the phonon characteristics are partly or fully resampled. In the case of dominant defects/impurity interactions only the propagation direction is resampled and the frequency remains unchanged. In the case of dominating $NU$ process, frequency and polarization are resampled according to the local temperature $\widetilde{T}$ with the modified distribution function $F_{scat}$ (Eq. (25)). The direction is only modified in the case of an umklapp interaction. More details about the selection rules used in this procedure can be found in [25].
- The simulation time is incremented by $\Delta t$ and the procedure restarts.

The probability for a phonon to be scattered between $t$ and $t + dt$ is

$$P_{scat}(\omega, p) = 1 - \exp\left(\frac{-\Delta t}{\tau(\omega, p)}\right) \tag{24}$$

The relaxation time $\tau(\omega, p)$ expression is slightly different from the one used with the KT technique. The boundary collision time $\tau_{BC}$ has not been used here since these interactions have already been taken into account during the drift stage exposed previously. Formal expression of $\tau_N$, $\tau_U$, $\tau_d$ and the related constants $A_p$, $B_p$ and $A$ have been derived from Holland's work [18].

In order to create phonons at the same rate they are destroyed at thermal equilibrium, the distribution function $F$ used to sample the frequencies of the phonons after scattering has to be modulated by the probability of scattering. So we define a new distribution function

$$F_{scat}(\widetilde{T}) = \frac{\sum_{j=1}^{i} N_j(\widetilde{T}) \times P_{scat\,j}}{\sum_{j=1}^{N_b} N_j(\widetilde{T}) \times P_{scat\,j}} \tag{25}$$

Taking into account the scattering probability in the distribution function $F_{scat}$ ensures that a destructed phonon on both transverse and longitudinal branches can be resampled with a not to weak energy. As it can be seen (Fig. 3), with the normalized cumulative distribution function $F_{scat}$, the sampled phonon distribution (red curve) is close to the theoretical one (for colours see the web version of this article).

With the MCM technique developed here, temperature can be known in each cell at every moments of the modeling through an inversion of the corresponding calculated energy $E^{\star}(T)$ using its theoretical form $E(T)$. Furthermore, the heat flux $\dot{q}$ in a given direction is the transported energy quanta flow moving at the group velocity. In the $z$ axis direction defined by vector $\mathbf{e}_z$ it can be written as

$$\dot{q}_z = \frac{1}{V} \sum_{n=1}^{N^{\star}(T)} W \hbar \omega_n \mathbf{v}_{gn} \cdot \mathbf{e}_z \tag{26}$$

If one can assume diffusive heat transport in the sample (i.e. $T > 100$ K and length $L$ sufficiently large to avoid ballistic effects), Fourier's law can be applied and the thermal conductivity $k_z$ is straightforwardly determined. If it is not the case, thermal conductance $G_z$ should be preferred since it takes into account the thickness $L$ of the sample

$$G_z = \frac{\dot{q}_z}{\Delta T} \xrightarrow[\text{Diffuse regime}]{} G_z = \frac{k_z}{L} \tag{27}$$

where $\Delta T$ is the temperature difference between the interfaces.

## 3. Bulk silicon thermal conductivity. Models validation

Comparison between silicon bulk data and the results given by the three methods, at temperatures between 100 and 500 K, have been achieved (Fig. 4). Experimental values have been taken in [47]. These measurements were performed on samples which characteristic length is equal to 7.16 mm.

At temperatures larger than 200 K, a weak dispersion in the thermal conductivity values obtained by the three methods can be noted. Furthermore there is a very good agreement between numerical predictions and experimental silicon bulk conductivity. The three methods and the parameters used in the modeling are validated in this temperature range.

At low temperatures, some discrepancies occur. Temperature shifts have been observed at the medium boundary for the DOM and MCM calculations, i.e. the diffusive regime is not completely reached in the case of studied samples. In the first case, the DOM solution has been obtained for a one millimeter size crystal. The temperature jump at boundaries leads to a weaker thermal gradient and thus to a larger thermal conductivity for the given heat flux. In the second case, MCM simulations have been performed on sub-millimeter sample size in order to have a reasonable computation time ($L \simeq 10$ µm). At this low temperature ballistic phonon behavior in thin structures seriously affects the thermal conductivity appraisal. As it will be shown later in this paper and in Appendix A, the concept of conductivity is questionable in this regime.

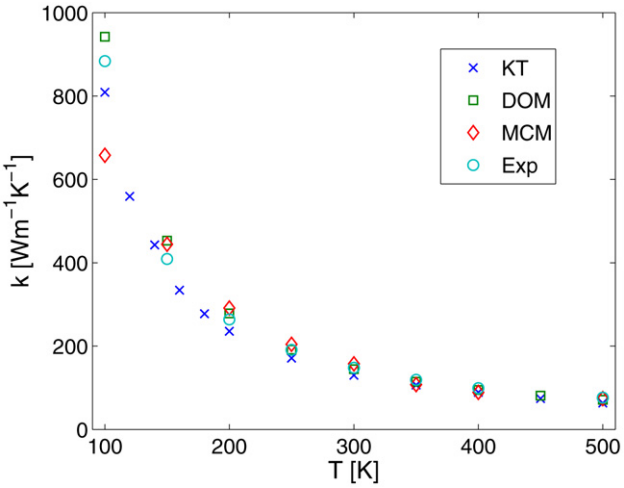


**Fig. 4.** Comparison of the bulk silicon thermal conductivity experimental data [47] at several temperatures with those obtained by the three numerical methods presented in the paper.

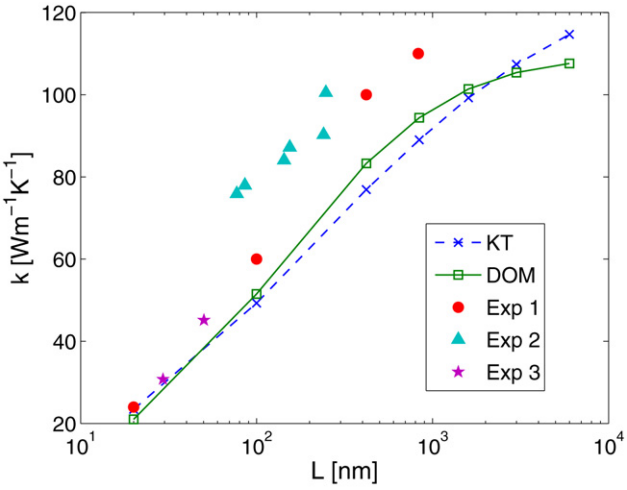


**Fig. 5.** In-plane thermal conductivity of silicon thin films at 300 K. KT model (dash line and cross), DOM model (full line and squares) and experimental data by: Ju and Goodson [9] (circles), Asheghi et al. [10] (triangles) and Liu and Asheghi [12] (stars).

## 4. Silicon in-plane thermal conductivity

The KT model has already been used to predict the in-plane thermal conductivity of silicon nanofilms of different thicknesses from 20 nm to 6 µm. A good agreement with experimental results in the temperature range between 20 to 300 K has been observed [19]. Here the DOM has been also used to make predictions of the in-plane thin film thermal properties. For the in-plane properties modeling the intensity boundary condition assumes perfectly diffuse scattering ($\rho^d = 1$ and $\rho^s = 0$). From the obtained intensity and temperature profiles it has been shown that films have a diffusive behavior if their thickness $L$ is much larger than the mean free path. At ambient temperature, the film thickness has to be larger than a few microns. At 300 K, in-plane thermal conductivities calculated with KT and DOM models agree very well. Moreover, they match quite well with experimental results for film thicknesses below 100 nm (Fig. 5). Above 100 nm, both models underestimate thermal conductivity by 20% which is a little bit higher than the experimental uncertainties (about 15%). Similar trends can be observe on other studies by MD considering very thin silicon films [49,50], in both cases in-plane thermal conductivity assessed by MD slightly over predict our simulation results. Lastly, results for

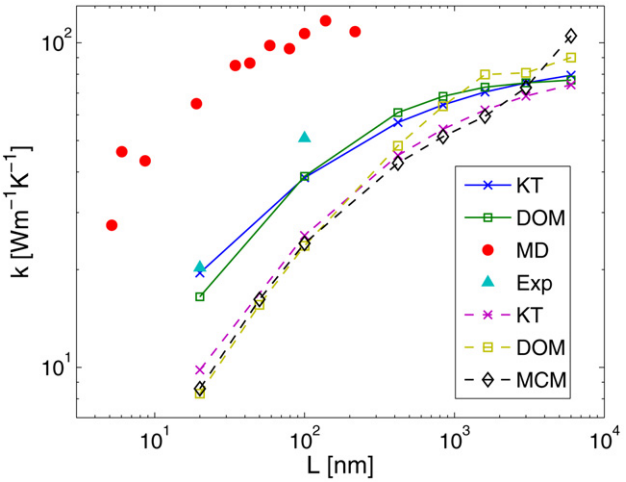


**Fig. 6.** Prediction of the in-plane thermal conductivity of Si nanofilms at 400 K obtained with KT model (full line and cross) and DOM model (full line and squares). Comparison with MD results by Gomes et al. [29] (circles), experiments by Liu and Asheghi [13] (triangles) and with an equivalent cross-plane thermal conductivity (dashed lines) from KT (cross), DOM (square) and MCM (diamonds) methods.

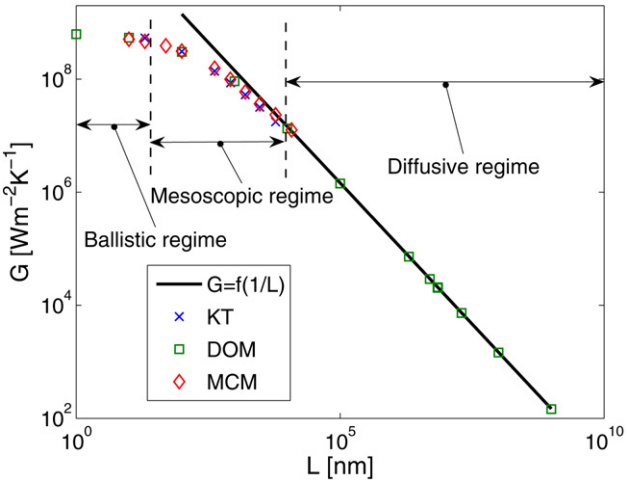


**Fig. 7.** Cross-plane conductance of silicon films of various thickness obtained at 300 K with DOM (squares), MCM (diamonds) and KT (cross) methods.

ultra-thin silicon layers where highly anisotropic effects might occurs due to phonon confinement can be found in Heino's work [51]. In this last case thermal conductivity is no longer the appropriate property and results are discussed in terms of thermal resistivity.

Our results have been also compared with the latest one obtained with MD simulations by Gomes et al. [29] at 400 K (Fig. 6). Once again, KT and DOM models agree well but differences are quite large (more than 100%) with MD simulations. Molecular Dynamics seems to lead to an overestimation of the thermal conductivity. Other comparisons with MD simulations [48,52] have been done at 300 K. They show a similar overestimation of MD simulations with respect to our methods and with experimental measurements [13]. No comparisons with the MCM model have been achieved for the in-plane modeling. In this last case the associated simulation involves huge computational resources that cannot be actually simply handled.

## 5. Silicon cross-plane thermal conductance

As it has been demonstrated, the KT and DOM methods succeed in the prediction of bulk and thin film in-plane thermal conductivities when compared to measurements. The MCM method also succeeds in predicting the thermal conductivity of bulk silicon. Thin film thermal conductivity measurements have been performed in the in-plane and cross-plane directions. Some cross-plane thermal conductivity measurements and calculations have been done for semiconductor superlattices or amorphous silicon films [5–8,53, 54]. No cross-plane thermal conductivity measurements have already been done for crystalline silicon films. The aim of this work is to predict this cross-plane thermal conductivity using the three models and to compare their results.

The MCM and DOM methods have shown that the temperature profile in a thin film is not always linear in steady state as predicted by Fourier's law which corresponds to the diffusive regime. When phonon mean free path is of the order of the film thickness, numerical simulations [25] point out that temperature jumps occur near the boundaries. The concept of conductivity, which in principle can only be used in the diffusion approximation, can lose its meaning for small film thickness. However, conductance can always be calculated. In the following, thermal conductance evaluations of silicon thin films of various thicknesses and temperatures will be presented. For both MCM and DOM methods the cross-plane properties modeling assumes perfectly smooth boundaries and thus only specular scattering ($\rho^d = 0$ and $\rho^s = 1$) to ensure momentum conservation.

In order to illustrate the limits of the conduction model at low scales, the cross-plane thermal conductance of silicon thin films at $T = 300$ K has been presented with a log–log representation in Fig. 7. At large thickness, conductance decreases as $1/L$ (where $L$ is the film thickness). This behavior is characteristic of a diffusive system. In this range, the concept of conductivity can be used. At very small thickness, conductance saturates: the transfer is purely ballistic. In between, the regime is "mesoscopic". The conductivity can hardly be used here. At ambient temperature, for film thickness lower than a few microns, heat transfer is no longer in the diffusive regime.

Contrary to the KT method, DOM and MCM do not suppose that the diffusive regime has been reached. As these two methods solve the full BTE in the relaxation time approximation, they should well describe the ballistic-mesoscopic-diffusive transition as long as phonon coherent effects do not play any role. Nevertheless, DOM calculations are faster when the sample characteristic length increases, while MCM calculations are penalized by the rising of sampled phonon number. Yet, it can be demonstrated (see Appendix A) that the KT presented here can correctly predict the equivalent thermal conductivity for the ballistic regime. Indeed, a collision time equal to the ratio of the system size to the phonon velocity has been introduced in the KT model. When this process is dominant toward the diffusion processes (i.e. when the mean free path associated with the boundary collision is smaller than the one associated with the diffusion processes phenomena), then the thermal conductivity depends linearly on the system size following equation (A.3). This leads to a thermal conductance which does not depend anymore on the system size as predicted by DOM and MCM models.

### 5.1. Thickness dependence

The cross-plane thermal conductance calculated at 400 K for a film thickness ranging from 20 nm to 6 μm has been presented in Fig. 8. The methods have been also compared to predictions made by Molecular Dynamics [29]. A good matching between our three methods can be noted, especially for large thickness, whereas the MD predictions give higher thermal conductances. Furthermore, a strong dispersion of the conductance is observed for layer thicknesses smaller than 40 nm in MD. In this width domain, our calcu-

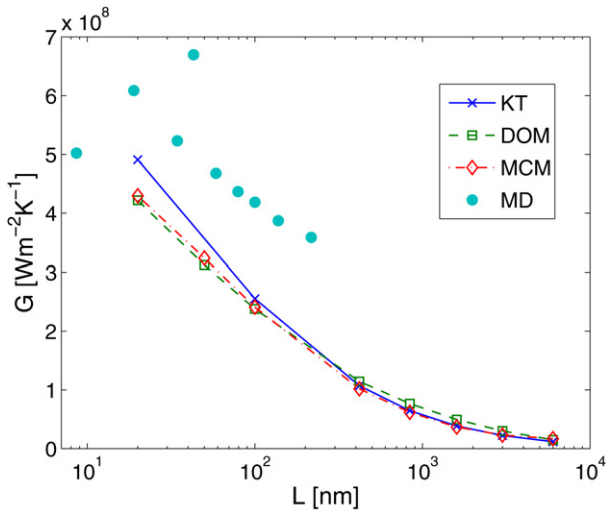


**Fig. 8.** Cross-plane thermal conductance of silicon thin film of various thicknesses at 400 K predicted with the three methods. Prediction of the MD by Gomes et al. [29] (circles) are also reproduced in the figure.

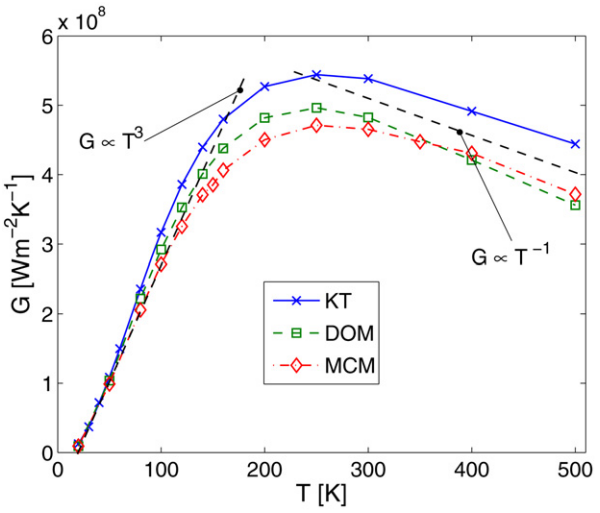


**Fig. 9.** Thermal conductance of a 20 nm thick silicon film versus temperature predicted by the three numerical methods. Low and high temperature conductance regime (dashed lined).

lations also exhibit a slight dispersion: in the mesoscopic regime, the KT model is indeed more questionable.

In Fig. 6, the equivalent cross-plane thermal conductivity (obtained by multiplying the conductance by the sample thickness) has been compared to the in-plane thermal conductivity. It can be noted that the equivalent cross-plane thermal conductivity is lower than the in-plane thermal conductivity, particularly at low thickness. Thermal conduction is therefore not isotropic in silicon crystalline films as it has also been observed in semiconductor superlattices [5]. Nevertheless, the anisotropy physical origin is very different in the film case and in the superlattice case. In the thin film situation, anisotropy is due to the fact that heat conduction is in a different regime in the in-plane situation (diffusive regime) and in the cross-plane situation (ballistic regime). In superlattices, cross-plane thermal transport can be reduced because band gaps are open in the phonon dispersion relation reducing the number of modes adequate to carry heat. But also due to the presence of interface diffuse reflection that increases contact resistance between layers [53]. Thus, film anisotropy has to be taken into account if heat transfer is simulated using classical Fourier's law. However, this kind of treatment has to be done carefully for thin films, since we pointed out that this approach should not be used for very thin films when heat transfer is not diffusive.

### 5.2. Temperature dependence

The cross-plane thermal conductance of a 20 nm-thick silicon film as function of the temperature has been plotted in Fig. 9. The agreement between our three methods is here again satisfactory. At low temperatures, the system is ballistic and the conductance simply depends on the thermal derivative of the phonon blackbody specific intensity (which is proportional to $T^4$) so that the conductance has a $T^3$ dependence. At high temperatures, the system enters in the diffusive regime: the mean free path is limited by anharmonic interactions so that the thermal conductance behaves as $1/T$. In the intermediate regime, the system is mesoscopic and requires a fine analysis as discussed in the three methods developed here. For example, the conductance maximum around 250 K is a compromise between the phonon relaxation time decrease with temperature and the phonon energy increase with temperature. Note that due to the same reasons, a similar conductance evolution with temperature, is actually observed in nanowire thermal conductivity measurements [55] and calculations [19,38,56].

## 6. Conclusions

In this paper three numerical methods used to predict cross-plane thermal conduction properties of thin silicon films have been presented. These three methods, Kinetic Theory, Discrete Ordinate Method and Monte Carlo Method, have been validated on their same prediction of silicon bulk thermal conductivity. Two models have been also validated comparing prediction values of the thin silicon film in-plane thermal conductivity with experimental values. The three methods agree very well regarding cross-plane thermal conduction properties. These models also agree with the few available experimental data. On the contrary, our models disagree with recent MD results that tend to overestimate the thermal conductivity. Each technique predicts a strong anisotropy of the thermal conduction properties, in-plane values being higher than cross-plane values. MCM and DOM have clearly shown the transition between diffusive and ballistic regime of phonon heat transfer. Thus, the concept of thermal conductivity can hardly be used in mesoscopic and ballistic regimes.

## Acknowledgements

The authors would like to thank Dr. Sebastian Volz (EM2C - École Centrale Paris), the *Thermique des Nanosystèmes et Nanomatériaux* GDR and the ANR contract ANR-JCJC-0180-01 for supporting this work.

## Appendix A

This appendix shows that the ballistic conductive heat flux, calculated between two parallel blackbodies, can be roughly retrieved by the Kinetic Theory if an appropriate mean free path is chosen. Let us consider as a simple illustration the following system

- the medium dispersion properties are acoustic modes which follow a single phonon branch in the Debye approximation [14],
- the medium is limited by plane parallel borders (orthogonal to $z$ direction) separated by a distance $L$ which are at temperatures $T_1$ and $T_2$ small compared to the Debye temperature.

In this approximation, the specific phonon intensity emitted by a wall at temperature $T$ reads

$$I^0(\omega) = \frac{\hbar\omega^3}{2\pi^3 v_g^2[\exp(\hbar\omega/k_bT) - 1]} \tag{A.1}$$

Here the group velocity $v_g$ is constant. The heat flux emitted by a wall at temperature $T_1$ is therefore

$$\dot{q} = \int_0^\infty d\omega \int_{\Omega=2\pi} I^0(\omega)\cos\theta\, d\Omega$$
$$= \frac{k_B^4}{2\pi^2 v_g^2 \hbar^3}\int_0^\infty \frac{x^3\,dx}{\exp(x)-1} T_1^4 = \sigma_{ph} T_1^4 \tag{A.2}$$

where $\theta$ is the angle between the direction $z$ and the direction of the intensity of consideration, $\sigma_{ph} = k_B^4\pi^2/(30\hbar^3 v_g^2)$.

The total heat flux exchanged is obtained by subtracting the heat flux emitted by the wall at temperature $T_2$ so that $\dot{q} = \sigma_{ph}(T_1^4 - T_2^4)$. If $T_1 \sim T_2 \sim T$, the total heat flux can be approximated by $\dot{q} \sim 4\sigma_{ph}T^3(T_1 - T_2)$. Following the definition of the thermal conductivity by the Fourier law, a ballistic conductivity along the $z$ direction can be written

$$k_z^{bal} = 4\sigma_{ph} L T^3 \tag{A.3}$$

Now, calculating the conductivity by the Kinetic Theory with Eq. (1) and doing the integration, one can write

$$k_z^{KT} = \int \tau v_z^2 C(\mathbf{K})\mathcal{D}(\mathbf{K})\, d^3\mathbf{K} \tag{A.4}$$

where $\mathcal{D}$ is the density of states. Thus, performing the integration over the angles and, after having changed the variables, over the angular frequencies $k_z$ becomes

$$k_z^{KT} = \int_0^{2\pi} d\phi \int_0^{\pi} \cos^2\theta \sin\theta\, d\theta \int_0^\infty \tau v_g^2 C(\omega)\frac{\omega^2\, d\omega}{2\pi^2 v^3}$$
$$= \frac{2\tau v_g k_B^4 T^3}{3\pi v_g^2 \hbar^3}\int_0^\infty \frac{x^4\exp(x)\,dx}{[\exp(x)-1]^2} = \frac{16\sigma_{ph} v_g \tau}{3\pi} T^3 \tag{A.5}$$

Thus, a mean free path taken as $\Lambda = v_g\tau = 3L/4\pi$ gives a Kinetic Theory thermal conductivity equal to the one obtained by a direct calculation of the ballistic heat flux.

## References


[1] R. Chau, B. Boyanov, B. Doyle, M. Doczy, S. Datta, S. Hareland, B. Jin, J. Kavalieros, M. Metz, Silicon nano-transistors for logic applications, Physica E 19 (1–2) (2003) 1–5.

[2] G. Chen, Phonon heat conduction in nanostructures, Int. J. Therm. Sci. 39 (2000) 471–480.

[3] D. Cahill, W. Ford, K. Goodson, G. Mahan, A. Majumdar, H. Maris, R. Merlin, S. Phillpot, Nanoscale thermal transport, J. Appl. Phys. 93 (2003) 793–818.

[4] W. Kim, R. Wang, A. Majumdar, Nanostructuring expands thermal limits, Nanotoday 2 (2007) 40–47.

[5] G. Chen, C. Tien, X. Wu, J. Smith, Thermal diffusivity measurement of GaAs/AlGaAs thin-film structures, J. Heat Transfer 116 (1994) 325–331.

[6] D. Cahill, M. Katiyar, J. Abelson, Thermal conductivity of a-si:h thin films, Phys. Rev. B 50 (9) (1994) 6077–6081.

[7] W. Capinski, H. Maris, T. Ruf, M. Cardona, E. Gmelin, K. Ploog, D.S. Katzer, Thermal-conductivity measurements of GaAs/AlAs superlattices using picosecond optical pump-and-probe technique, Phys. Rev. B 59 (12) (1999) 8105–8113.

[8] R. Venkatasubramanian, Lattice thermal conductivity reduction and phonon localization like behavior in superlattice structures, Phys. Rev. B 61 (4) (2000) 3091–3097.

[9] Y. Ju, K. Goodson, Phonon scattering in silicon films with thickness of order 100 nm, Appl. Phys. Lett. 74 (20) (1999) 3005–3007.

[10] M. Asheghi, M. Toulzebaev, K. Goodson, Y. Leung, S. Wong, Temperature-dependent thermal conductivity of single-crystal silicon layers in SOI substrates, J. Heat Transfer 120 (1) (1998) 30–36.

[11] W. Liu, M. Asheghi, Phonon-boundary scattering in ultrathin single-crystal silicon layers, Appl. Phys. Lett. 84 (19) (2004) 3819–3821.

[12] W. Liu, M. Asheghi, Thermal conduction in ultrathin pure and doped single-crystal silicon layers at high temperatures, J. Appl. Phys. 98 (12) (2005) 123523.

[13] W. Liu, M. Asheghi, Thermal conductivity measurements of ultra-thin single crystal silicon layers, J. Heat Transfer 128 (1) (2006) 75–83.

[14] C. Kittel, Introduction to Solid State Physics, 8th edition, John Wiley and Sons, Philadelphia, 2004.

[15] P. Klemens, The thermal conductivity of dielectric solids at low temperatures (theoretical), Proc. Roy. Soc. A 208 (1092) (1951) 108–133.

[16] P. Klemens, Solid State Physics, vol. 7, Academic Press Inc., New York, 1958.

[17] J. Callaway, Model for lattice thermal conductivity at low temperatures, Phys. Rev. 113 (1959) 1046–1051.

[18] M. Holland, Analysis of lattice thermal conductivity, Phys. Rev. 132 (6) (1963) 2461–2471.

[19] P. Chantrenne, J. Barrat, X. Blase, J. Gale, An analytical model for the thermal conductivity of silicon nanostructures, J. Appl. Phys. 97 (2005) 104318.

[20] A. Majumdar, Microscale heat conduction in dielectric thin films, J. Heat Transfer 115 (1993) 7–16.

[21] M. Modest, Radiative Heat Transfer, 2nd edition, Academic Press, San Diego, 2003.

[22] D. Lemonnier, Microscale and Nanoscale Heat Transfer, Topics in Applied Physics, vol. 107, Springer, Berlin, 2007, pp. 77–106 (Ch. 5).

[23] G. Chen, Thermal conductivity and ballistic phonon transport in cross-plane direction of superlattices, Phys. Rev. B 57 (23) (1998) 14958–14973.

[24] S. Volz, D. Lemonnier, J.-B. Saulnier, Clamped nanowire thermal conductivity based on phonon transport equation, Microscale Thermophys. Eng. 5 (3) (2001) 191–207.

[25] D. Lacroix, K. Joulain, D. Lemonnier, Monte Carlo transient phonon transport in silicon and germanium at nanoscales, Phys. Rev. B 72 (2005) 064305.

[26] R. Peterson, Direct simulation of phonon-mediated heat transfer in a Debye crystal, J. Heat Transfer 116 (4) (1994) 815–822.

[27] S. Mazumder, A. Majumdar, Monte Carlo simulations of phonon transport in solid thin films including dispersion and polarization, J. Heat Transfer 123 (2001) 749–759.

[28] S. Volz, G. Chen, Molecular dynamics simulation of thermal conductivity of silicon nanowires, Appl. Phys. Lett. 75 (1999) 2056–2058.

[29] C. Gomes, M. Madrid, J. Goicochea, C. Amon, In plane and out of plane thermal conductivity of si thin films predicted by molecular dynamics, J. Heat Transfer 128 (2006) 1114–1121.

[30] J. Chung, A. Mc Gaughey, M. Kaviany, Role of phonon dispersion in lattice thermal conductivity modeling, J. Heat Transfer 126 (3) (2004) 376–380.

[31] P. Chantrenne, J. Barrat, Finite size effects in determination of thermal conductivities: comparing molecular dynamics results with simple models, J. Heat Transfer 126 (2004) 577–585.

[32] P. Flubacher, A. Leadbetter, J. Morrison, The heat capacity of pure silicon and germanium and properties of their vibrational frequency spectra, Phil. Mag. 4 (39) (1959) 273–294.

[33] M. Holland, Phonon scattering in semiconductors from thermal conductivity studies, Phys. Rev. 134 (2A) (1964) A471–A480.

[34] X. Lu, J. Chu, Modification of the lattice thermal conductivity in semiconductor rectangular nanowires, J. Appl. Phys. 93 (2) (2003) 1219.

[35] J. Zou, A. Balandin, Phonon heat conduction in a semiconductor nanowire, J. Appl. Phys. 89 (5) (2001) 2932–2938.

[36] I. Rosenblum, J. Adler, S. Brandon, Calculation of thermal properties of diamond from simulated phonon spectra, Comput. Mater. Sci. 12 (1998) 9–25.

[37] H. Casimir, Note on the conduction of heat in crystals, Physica 5 (1938) 495–500.

[38] N. Mingo, Calculation of si nanowire thermal conductivity using complete phonon dispersion relations, Phys. Rev. B 68 (11) (2003) 113308.

[39] S.V.J. Narumanchi, J.Y. Murthy, C. Amon, Submicron Heat transport model in silicon accounting for phonon dispersion and polarization, J. Heat Transfer 126 (2004) 946–955.

[40] S. Usher, G. Srivastava, Theoretical study of the anharmonic decay of nonequilibrium LO phonons in semiconductor structures, Phys. Rev. B 50 (1994) 14179–14186.

[41] S. Chandrasekhar, Radiative Transfer, Dover, New York, 1960.

[42] W. Fiveland, A discrete ordinate method for predicting radiative heat transfer in axisymmetric enclosures, ASME paper 82-HTD-20.

[43] D. Lemonnier, M. Lallemand, Heat transfer at time and space microscales by radiative phonon transport modelling, Int. J. Heat Technology 18 (Suppl. 1) (2000) 63–68.

[44] D. Terris, K. Joulain, D. Lacroix, D. Lemonnier, Modeling semi-conductor thermal properties. The dispersion role, Submitted in January 2008, URL http://arxiv.org/abs/0803.3954.

[45] E. Pop, R. Dutton, K. Goodson, Analytic band Monte Carlo model for electron transport in Si including acoustic and optical phonon dispersion, J. Appl. Phys. 96 (2004) 4998–5005.
[46] G. Dolling, Lattice vibration in crystals with diamond structures, in: I. Vienna (Ed.), Symposium on Inelastic Scattering Neutrons in Solids and Liquids, vol. 2, Chalk River, 1963, pp. 37–48.
[47] C.J. Glassbrenner, G.A. Slack, Thermal conductivity of silicon and germanium from 3 k to the melting point, Phys. Rev. 134 (1964) A1058–A1069.
[48] X.-L. Feng, Molecular dynamics simulation of thermal conductivity of nanoscale thin silicon films, Nanoscale Microscale Thermophys. Engrg. 7 (2) (2003) 153–161.
[49] Z. Li, P. Xiao, Molecular dynamic simulation and theoretical study on in-plane thermal conductivity of single crystal silicon film at nanoscale, in: Proc. of the 13th Int. Heat. Trans. Conf., Sydney, Australia, 2006, pp. NAN-10.
[50] W. Zenghui, L. Zhixin, Lattice dynamics analysis of thermal conductivity in silicon nanoscale film, Appl. Therm. Engrg. 26 (2006) 2063–2066.
[51] P. Heino, Dispersion and thermal resistivity in silicon nanofilms by molecular dynamics, Eur. Phys. J. B 60 (2007) 171–179.
[52] W. Zenghui, L. Zhixin, Research on the out-of-plane thermal conductivity of nanometer silicon film, Thin Solid Films 515 (4) (2006) 2203–2206.
[53] B. Yang, G. Chen, Partially coherent phonon heat conduction in superlattices, Phys. Rev. B 67 (2003) 195311.
[54] B. Yang, G. Chen, Experimental studies on thermal conductivity of thin films and superlattice materials, in: T. Tritt (Ed.), Thermal Conductivity, Kluwer Press, 2007, pp. 167–186.
[55] D. Li, Y. Wu, P. Kim, P. Yang, A. Majumdar, Thermal conductivity of individual silicon nanowires, Appl. Phys. Lett. 83 (14) (2003) 2934–2936.
[56] D. Lacroix, K. Joulain, D. Terris, D. Lemonnier, Monte Carlo transient phonon transport in silicon and germanium at nanoscales, Appl. Phys. Lett. 89 (2006) 103104.